Journal of Geophysical Research: Atmospheres

RESEARCH ARTICLE
10.1029/2017JD028028

The Impacts of Chinese Wind Farms on Climate

Hongwei Sun[1], Yong Luo[1], Zongci Zhao[1], and Rui Chang[1,2]

[1]Ministry of Education Key Laboratory for Earth System Modeling, Department of Earth System Science, Tsinghua University, Beijing, China, [2]Public Meteorological Service Center, CMA, Beijing, China

Key Points:
- A new wind farm fleet scenario, representing Chinese wind energy development level in 2015, is designed to study its climatic impacts
- Momentum sink and turbulent kinetic energy source caused by wind farms are first separated to evaluate their respective climatic impacts
- Wind farms could impact local and regional climate, causing changes in both lower-level and upper-level atmosphere over specific areas

Supporting Information:
- Supporting Information S1
- Table S1

Correspondence to:
Y. Luo,
yongluo@mail.tsinghua.edu.cn

Citation:
Sun, H., Luo, Y., Zhao, Z., & Chang, R. (2018). The impacts of Chinese wind farms on climate. *Journal of Geophysical Research: Atmospheres*, *123*, 5177–5187. https://doi.org/10.1029/2017JD028028

Received 19 NOV 2017
Accepted 5 APR 2018
Accepted article online 16 APR 2018
Published online 27 MAY 2018

Abstract As a renewable energy resource, wind energy has developed fast in recent years, and its impacts on climate have received widespread attention. In this study, a new wind farm fleet scenario is designed based on Chinese wind farm data from the Chinese Wind Energy Association and Chinese cumulative wind power capacity data from the Global Wind Energy Council. A mesoscale numerical model is used to simulate the impacts of wind farms on climate. The results indicate that the wind farms in the designed scenario could impact the local and regional climate in China, causing changes in both lower-level atmosphere (changes within ±0.5 K for 2-m temperature) and upper-level atmosphere (changes within ±30 m^2/s^2 for 500-hPa geopotential height) over several specific areas. The momentum sink and the turbulent kinetic energy source generated by wind farms are first separated to evaluate their respective contributions to the impacts of wind farms on climate.

Plain Language Summary With the rapid development of wind energy, the impacts of wind farms on environment have attracted increasing attention. A new wind farm fleet scenario is designed in the study to analyze the climatic impacts of wind farms in China. The results show the local and regional climatic impacts of wind farms in China (e.g., changes within ±0.5 K for 2-m temperature and ± 30 m^2/s^2 for 500-hPa geopotential height), which are much smaller than the interannual climate variability. This research can provide China, as well as other countries and regions, with useful scientific advice for the environment-friendly development of wind energy.

1. Introduction

It is known that global power consumption keeps growing at present; the global primary energy consumption reaches up to 13,276.3 Mtoe (≈154,403.4 TWh) in 2016 (BP, 2017). And because fossil fuels are gradually being exhausted and cause serious environmental problems, renewable energy resources are now receiving increasing attention. Wind energy, one of the renewable energy resources that do not emit gases during the energy generation process, is currently in a stage of rapid development. According to the data from the Global Wind Energy Council (2017), the global cumulative installed wind power capacity was 486,749 MW until 2016. And China ranked first among all countries worldwide in terms of new installed wind power capacity, as well as cumulative wind power capacity, in 2016. Chinese National Energy Bureau reported that Chinese wind power production was 185.6 TWh in 2015, increased by 16.17% compared with the wind power production in 2014. Thus, wind power production in China is quantitatively large and undergoing rapid development. According to the proposal for the thirteenth Five-Year Plan issued by the Chinese National Energy Bureau, the wind power capacity in China will maintain an annual growth rate of 9.9% over the next five years (2015–2020). Wind energy in China will continue to develop rapidly in the future.

With the rapid development of wind energy, the impacts of wind farms on local and regional weather and climate have attracted increasing attention. Several studies have found that wind farms can significantly decrease wind speed at the hub height of wind turbines within and downwind of wind farms (Baidya Roy et al., 2004; Fitch et al., 2013; Hasager et al., 2015; Smith et al., 2013). Observations have shown a clear wind speed wake from the wind farm installed in the Midwestern United States at a distance of 190 m or 2.4 rotor diameters (Smith et al., 2013). Fitch et al. (2013) parameterized a 10-km × 10-km wind farm in the Weather Research and Forecasting (WRF) model to study its mesoscale influence on the atmosphere in a diurnal cycle. The results indicated a significant impact on the local atmospheric flow and on regions up to 60 km downwind at night. Studies also show that wind farms can influence temperatures within wind farms, as well as over large areas around wind farms (Baidya Roy & Traiteur, 2010; Chang et al., 2016; Walsh-Thomas et al., 2012; Zhou et al., 2012). Baidya et al. (2010) analyzed temperature data from a wind farm at San Gorgonio

and found that the wind farm had a warming effect during the night and a cooling effect during the day, which resulted from enhanced vertical mixing due to turbulence generated by wind turbine rotors. Chang et al. (2016) analyzed Moderate Resolution Imaging Spectroradiometer land surface temperature (LST) data during the period of 2005–2012. They identified noticeable nighttime warming trends in LSTs within wind farm areas relative to nearby non–wind farm regions in Guazhou, which is located in northwestern China. According to the study, the nighttime LST warming is strongest in summer (0.51 °C/8 years). Other studies also suggest that wind farms have significant impacts on precipitation, sea level pressure, and so on (Barrie & Kirk-Davidoff, 2010; Fiedler & Bukovsky, 2011; Vautard et al., 2014; C. Wang & Prinn, 2010). Vautard et al. (2014) employed a regional climate model to describe the interactions between turbines and the atmosphere. They found a statistically significant signal in winter, with changes within 0–5% for precipitation and ± 0.5 hPa for sea level pressure. Therefore, even though wind energy plays an important role in reducing both fossil fuel combustion and greenhouse gas emissions, it is still necessary to obtain a clear understanding of wind farms' impacts on weather and climate.

In this study, a new wind farm fleet scenario is designed to represent the Chinese wind energy development level in 2015. The wind turbines in this designed scenario are parameterized as a momentum sink and a turbulent kinetic energy (TKE) source (Fitch et al., 2012) in a WRF (Skamarock et al., 2008) to study their impacts on climate. To obtain a deeper understanding of the interactions between wind farms and the atmosphere, we separate the momentum sink and TKE source in wind turbine parameterization to evaluate their respective contributions to the climatic impacts of wind farms. The research is expected to provide China, as well as other countries and regions, with useful scientific advice for the environment-friendly development of wind energy.

2. Experimental Method

2.1. Model Experiments

In this study, the WRF model is used to simulate the impacts of wind farms on climate under the designed Chinese wind farm fleet scenario in 2015. Figure 1 shows the simulated domain, which covers the mainland of China and some coastal areas. The shading represents the topography, and the purple dots represent wind farms. Sixteen 1-year simulations are carried out within the period extending from March (this year) to February (next year), and the initial and boundary conditions of each simulation are supplied by 1° × 1° final (FNL) data in different years (2000–2015) from the National Centers for Environmental Prediction. The simulation has a horizontal resolution of 30 km. There are 32 eta levels in the vertical direction, including 3 levels intersecting the turbine rotor area and 10 levels under 1 km. In addition, the MYNN2.5 and Noah schemes are used to represent the planetary boundary layer physics and the land surface, respectively.

2.2. Wind Energy Development Scenario

The wind farm fleet scenario designed in the study includes 722 wind farms, which are shown as purple dots in Figure 1. The Chinese wind farm data (number and locations of the wind farms) used in the designed scenario are provided by the Chinese Wind Energy Association (CWEA). In order to simplify the simulation, (1) each wind farm contains 100 wind turbines; (2) both the rotor diameter and the hub height of each wind turbine are 100 m; (3) the cut-in and cut-out wind speeds are 4 m/s and 25 m/s, respectively; (4) the WRF default power curve in the Fitch module is used for each wind turbine here; (5) the nominal power of each turbine is 2 MW. Thus, the total power capacity in the designed scenario is 144,400 MW, which is close to the Chinese cumulative wind power capacity (145,362 MW) in 2015 provided by the Global Wind Energy Council (2017). On the one hand, compared with previous studies that adopted idealized wind farm fleet scenarios (in which, e.g., all of the wind farms are grouped together), the wind farm fleet scenario designed in this study provides a better representation of Chinese wind energy development level in 2015 (based on its real number and locations of wind farms and its similar cumulative wind power capacity to the reality). On the other hand, the simplification used to represent wind farms in the simulations determines that the designed wind farm fleet scenario cannot perfectly represent the actual wind farms in China. Therefore, the wind farm fleet scenario designed in this study provides a better, but not perfect, representation of Chinese wind energy development level in 2015.

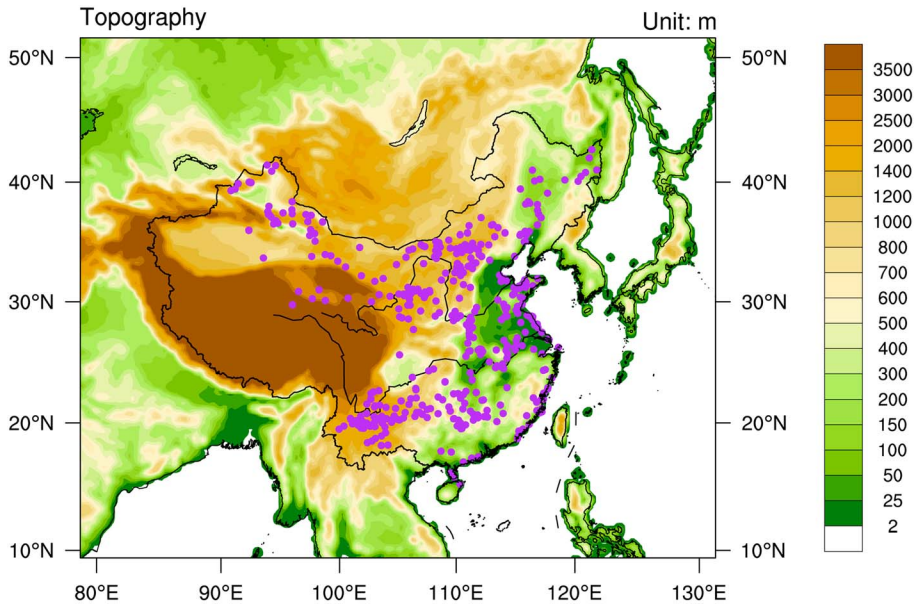

Figure 1. Topography (shaded) of the simulated domain and the locations of wind farms (purple dots).

2.3. Simulation Characteristics and Evaluation

Three simulations are carried out in the study, which are summarized in Table 1. No wind turbines are employed in the CTL simulation. SCEN1 and SCEN2 simulations employ wind turbines under the designed wind farm fleet scenario (described in section 2.2). The difference between SCEN1 and SCEN2 is the following: wind turbines in SCEN1 are parameterized as both the momentum sink and TKE source in the Fitch module (Fitch et al., 2012), whereas the wind turbines in SCEN2 are parameterized as only the momentum sink (the TKE source in the Fitch module is modified to be a constant, which is 0). Therefore, the total impacts of wind farms on climate are reflected by the differences between SCEN1 and CTL. The contributions of momentum sink to the climatic impacts of wind farms can be determined by comparing SCEN2 and CTL; the contributions of the TKE source to the climatic impacts of wind farms can be determined by comparing SCEN1 and SCEN2. It should be pointed out that, only when the climatic impacts of the two components (momentum sink and TKE source) in the wind turbine parameterization are linearly additive, the differences between SCEN1 and SCEN2 exactly represent the contributions of TKE source to the climatic impacts of wind farms. Thus, we should note that even though we consider the differences between SCEN1 and SCEN2 as the climatic impacts of TKE source here, the nonlinear interactions between momentum sink and TKE source also contribute to the differences between SCEN1 and SCEN2.

The climatic means (temporal mean of the 16-year simulated period from March 2000 to February 2016) of several variables (T2, wind-10 m, P-sfc, and HGT500 shown in Table 2) in the CTL simulation data and European Centre for Medium-Range Weather Forecasts Re-Analysis (ERA)-Interim reanalysis data ($0.25° \times 0.25°$) are calculated to evaluate the simulating effects of CTL. Figure 2 shows that the climatic means of 2-m temperature in CTL simulation results (Figure 2a) and ERA-Interim reanalysis data (Figure 2c) have very similar spatial distributions (the spatial correlation coefficient is 0.990). And there exists a systematic

Table 1
Summary of Simulations Characteristics

Simulation	Wind farms	Wind turbine parameterization
CTL	No wind farms	
SCEN1	With 722 wind farms	As both the momentum sink and TKE source
SCEN2	With 722 wind farms	As only the momentum sink

Note. TKE = turbulent kinetic energy.

Table 2
Spatial Correlations and Regional Averaged Differences (CTL-ERA) of Several Variables Between CTL and ERA-Interim

	T2	Wind-10 m	P-sfc	HGT500
Correlation	0.990[a]	0.938[a]	0.999[a]	0.997[a]
Difference	−2.673 K	0.196 m/s	0.089 hPa	28.047 gpm

Note. T2 = 2-m temperature; Wind-10 m = 10-m horizontal wind speed; P-sfc = surface pressure; HGT500 = 500-hPa geopotential height; ERA = European Centre for Medium-Range Weather Forecasts Re-Analysis.
[a]Means the correlation passes the 99% confidence level.

deviation of 2-m temperature between CTL and ERA (the difference of regional averaged 2-m temperature between CTL and ERA in Figure 2 is −2.673 K). Since CTL is driven by FNL reanalysis data, this 2-m temperature systematic deviation (−2.673 K) between CTL and ERA mainly results from the systematic deviation between FNL and ERA (the difference of regional averaged 2-m temperature between FNL and ERA in Figure 2 is −2.120 K). Other variables, including 10-m horizontal wind speed, surface pressure, and 500-hPa geopotential height, also show high similarity between CTL and ERA (see Table 2). Therefore, the CTL simulation results are generally similar to the ERA-Interim reanalysis data and can be used to study the effects of wind farms on climate.

2.4. Data and Methods

All the analyses in this study are based on the monthly mean data calculated from the simulation results. For example, Figure 4 shows the impacts of the wind farms on regional climate. Summer (left column in Figure 4) represents the summer months (June, July, and August) from 2000 to 2015 (48 months in total), and winter (right column in Figure 4) represents the winter months (December, January, and February) from 2000 to 2015 (December 2000 to February 2016, 48 months in total). More specifically, Figure 4a shows the difference of summer mean (average of all the summer months from 2000 to 2015) 2-m temperature between SCEN1 and CTL.

A contrast experiment t test formulation ($t = \frac{\overline{d}}{s_D/\sqrt{n}}$) is adopted to test the significance of the atmospheric changes caused by wind farms (such as crosshatched lines in Figure 4a). For example, each grid point in Figure 4a has a time series, which contains 48 values (June, July, and August from 2000 to 2015) that represent the monthly mean 2-m temperature in SCEN1 ($T_1^{\mathrm{SCEN1}}, T_2^{\mathrm{SCEN1}}, \ldots, T_{48}^{\mathrm{SCEN1}}$) or CTL ($T_1^{\mathrm{CTL}}, T_2^{\mathrm{CTL}}, \ldots, T_{48}^{\mathrm{CTL}}$). A time series ($T^d$), which represents the difference between monthly mean 2-m temperature in SCEN1 and CTL, is calculated based on $T_i^d = T_i^{\mathrm{SCEN1}} - T_i^{\mathrm{CTL}}, i = 1, 2, \ldots, 48$. For the t test applied in each grid point in Figure 4a

$$t = \frac{\overline{d}}{s_D/\sqrt{n}}$$

n = 48 represents the number of summer months (June, July, and August from 2000 to 2015);

$\overline{d} = \frac{1}{n}\sum_{i=1}^{n} T_i^d$ represents the mean value of the time series T^d; and

$s_D = \sqrt{\frac{1}{n}\sum_{i=1}^{n}\left(T_i^d - \overline{d}\right)^2}$ represents the standard deviation of the time series T^d.

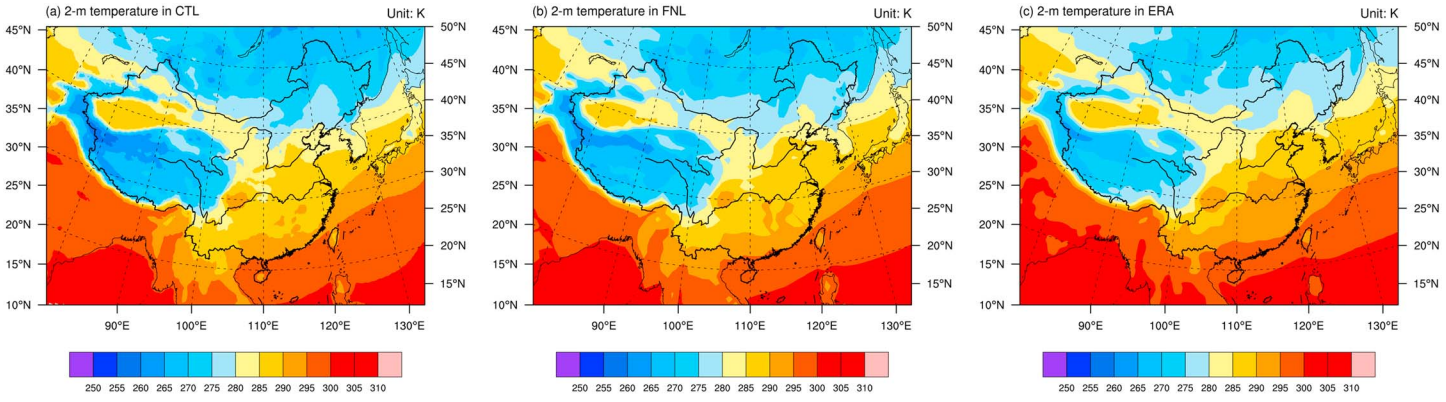

Figure 2. Climatic means of 2-m temperature in the (a) CTL simulation, (b) FNL reanalysis data, and (c) ERA-Interim reanalysis data during 2000–2015. FNL = final; ERA = European Centre for Medium-Range Weather Forecasts Re-Analysis.

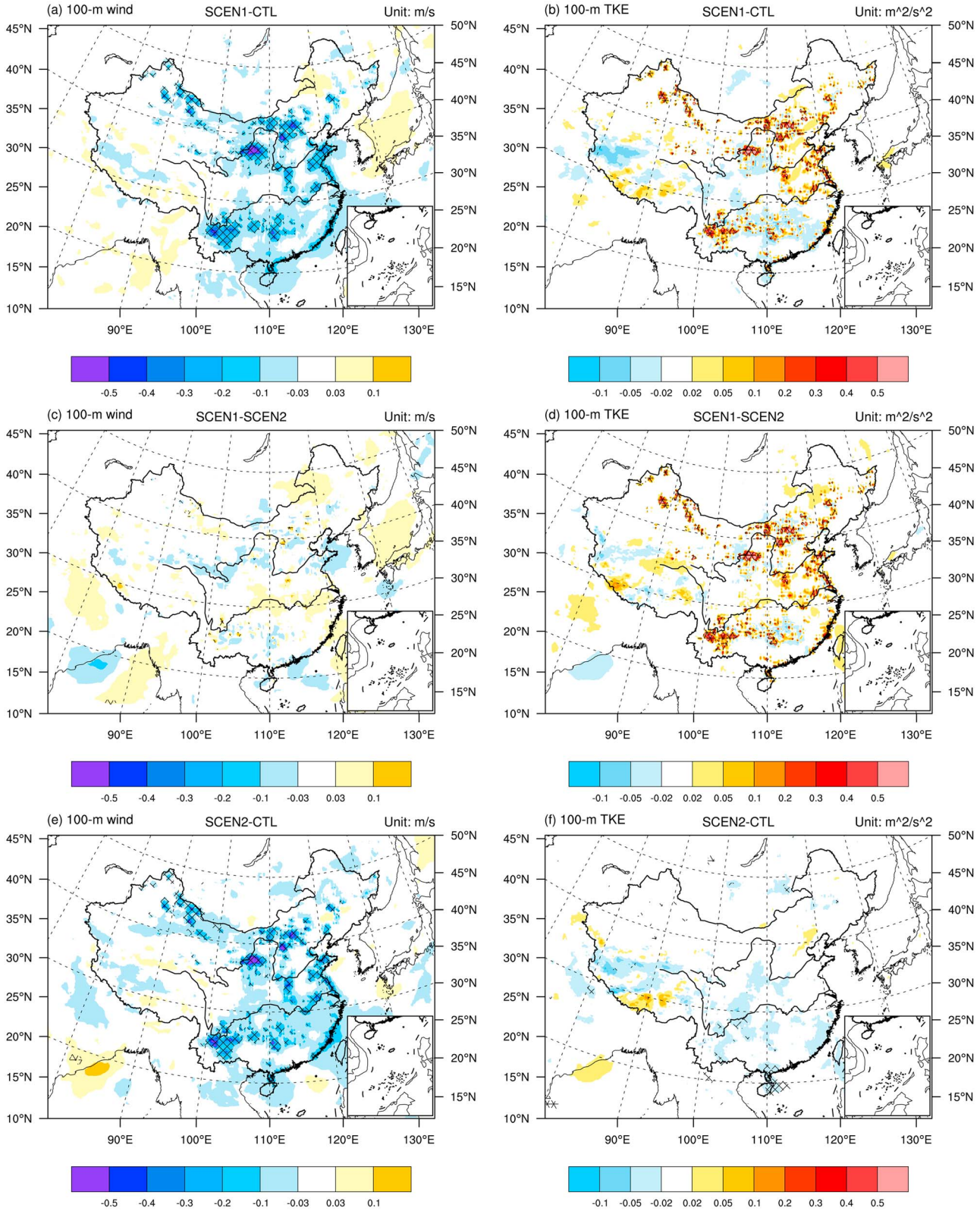

Figure 3. Differences in climatic mean (a, c, e) horizontal wind speed and (b, d, f,) turbulent kinetic energy at hub height (100 m) between different simulations. Regions with 95% confidence level of differences (calculated based on the contrast experiment t test formulation $t = \frac{\overline{d}}{s_D/\sqrt{n}}$) are highlighted with crosshatched lines. TKE = turbulent kinetic energy.

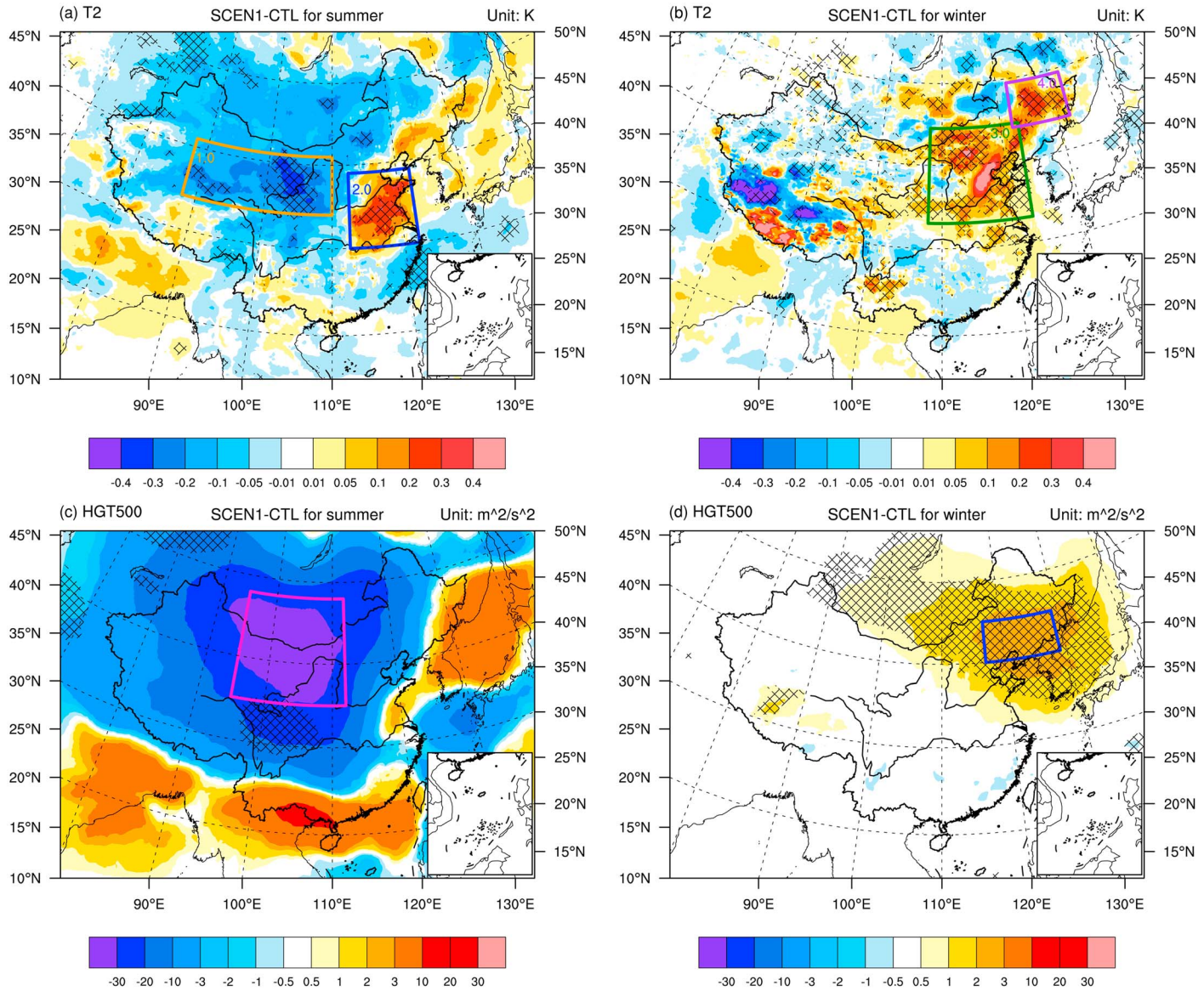

Figure 4. Mean differences in (a, b) 2-m temperature and (c, d) 500-hPa geopotential height between SCEN1 and CTL in summer (June, July, and August) and winter (December, January, and February). Regions with 95% confidence level of differences (calculated based on the contrast experiment t test formulation $t = \frac{\bar{d}}{s_D/\sqrt{n}}$) are highlighted with crosshatched lines.

The t value (calculated based on $t = \frac{\bar{d}}{s_D/\sqrt{n}}$ above) in each grid point would be compared with $t_{0.05}(n) = 2.0$, $n = 48$ to determine the grid points with 95% confidence level of differences.

3. Results

3.1. Local Climatic Impacts of Wind Farms

Figures 3a and 3b show that wind farms have statistically significant impacts on 100-m horizontal wind speed and 100-m TKE. The impacts of wind farms on wind speed and TKE at hub height are generally local impacts since the changes of 100-m horizontal wind speed (Figure 3a) and 100-m TKE (Figure 3b) mainly occur around the locations of wind farms (Figure 1). This is different from the impacts of wind farms on 2-m temperature and 500-hPa geopotential height, which are considered as regional climatic impacts (shown in section 3.2),

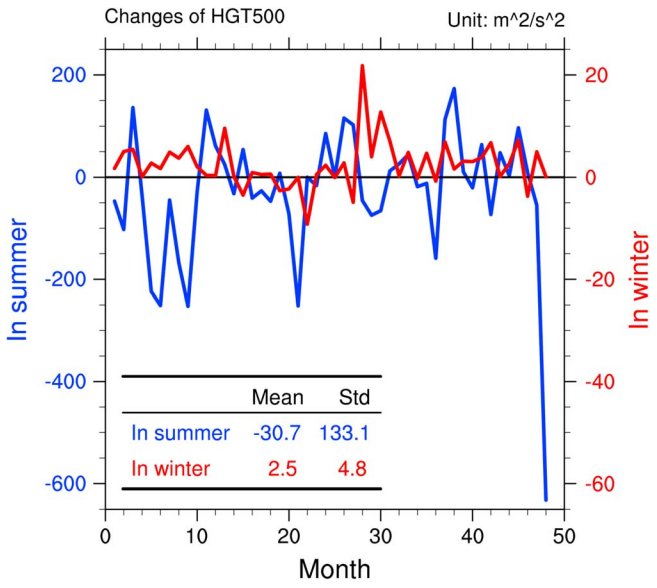

Figure 5. Time series of the regional averaged changes in HGT500 caused by wind farms over the selected areas (red box in Figure 4c and blue box in Figure 4d). The *x* axis represents the number of summer months (June, July, and August from 2000 to 2015; 48 months in total) for the blue curve, as well as the number of winter months (December, January, and February from 2000 to 2015, 48 months in total) for the red curve. "Mean" represents the temporal mean of the curve; "Std" represents the standard deviation of the curve.

because the changes in 2-m temperature and 500-hPa geopotential height caused by wind farms are more centralized and are not exactly around the locations of wind farms like changes in 100-m horizontal wind speed and 100-m TKE.

Figure 3d shows statistically significant increase of 100-m TKE, which is similar to Figure 3b, whereas there is tiny changes in 100-m horizontal wind speed in Figure 3c. On the contrary, Figure 3e shows statistically significant decreases of 100-m horizontal wind speed, which is similar to Figure 3a, whereas there is tiny changes of 100-m TKE in Figure 3f. Obviously, these tiny changes of 100-m horizontal wind speed in Figure 3c, which may result from the redistribution of wind speed caused by the increase of TKE, are much smaller than the changes of 100-m horizontal wind speed in Figure 3e; the tiny changes of 100-m TKE in Figure 3f, which may result from the changes of vertical wind shear caused by the momentum sink, are much smaller than the changes of 100-m TKE in Figure 3d. Therefore, the momentum sink (causes changes in 100-m horizontal wind speed) and TKE source (causes changes in 100-m TKE) in the wind turbine parameterization are successfully separated in general.

3.2. Regional Climatic Impacts of Wind Farms

Figure 4 shows the impacts of wind farms on 2-m temperature (Figures 4a and 4b) and 500-hPa geopotential height (Figures 4c and 4d). A statistically significant increase in 2-m temperature is noted in the eastern coastal area in summer, and the maximum increase is ~0.2 K (blue box in Figure 4a). A statistically significant decrease in 2-m temperature occurs over a large Chinese inland area in summer, and the maximum decrease in temperature is ~0.3 K (orange box in Figure 4a). In winter, a wide area of warming occurs in northeast China (green and purple boxes in Figure 4b), and the greatest warming reaches more than 0.4 K. Moreover, we examine the 500-hPa geopotential height (HGT500) to analyze the wind farms' effects on the high-level atmosphere. Figures 4c and 4d show that wind farms could cause high-level atmospheric changes, with negative anomalies in HGT500 over Chinese inland areas in summer and positive anomalies in HGT500 over northeast China in winter. It is also interesting to note that even though the decrease in HGT500 over Chinese inland areas in summer is much larger than the increase of HGT500 over northeast China in winter, this larger decrease of HGT500 in summer (red box in Figure 4c) does not pass 95% confidence level, whereas the smaller increase of HGT500 in winter (blue box in Figure 4d) passes 95% confidence level.

To explain this phenomenon, the regional averaged HGT500 changes in the selected areas (red box in Figure 4c and blue box in Figure 4d) are calculated (Figure 5). The temporal average of the blue curve ($-30.7\ m^2/s^2$), which represents the changes of HGT500 in summer, is much greater than the temporal average of the red curve ($2.5\ m^2/s^2$), which represents the changes of HGT500 in winter. Meanwhile, the fluctuations of the blue curve over time are larger than those of the red curve, which is consistent with the statistical results that the standard deviation of the blue curve ($133.1\ m^2/s^2$) is much larger than that of the red curve ($4.8\ m^2/s^2$). In addition, the values represented by the red curve are generally positive. These results show that the changes in HGT500 caused by wind farms are larger and fluctuate dramatically in summer, so they could not pass 95% confidence level. The changes in HGT500 caused by wind farms are smaller in winter but are primarily positive in value and have much smaller fluctuations, which determines that the HGT500 changes in winter pass 95% confidence level. This result means that even a very small change ($\overline{d}$) could be statistically significant if its standard deviation (s_D) is also very small (like the red curve in Figure 5), a large change may not be statistically significant if its standard deviation is also very large (like the blue curve in Figure 5), according to $t = \dfrac{\overline{d}}{s_D/\sqrt{n}}$.

In winter, the increase of 2-m temperature (Figure 4b) and the increase of 500-hPa geopotential height (Figure 4d) are both located over northeast China. Previous studies have suggested that the East Asian trough

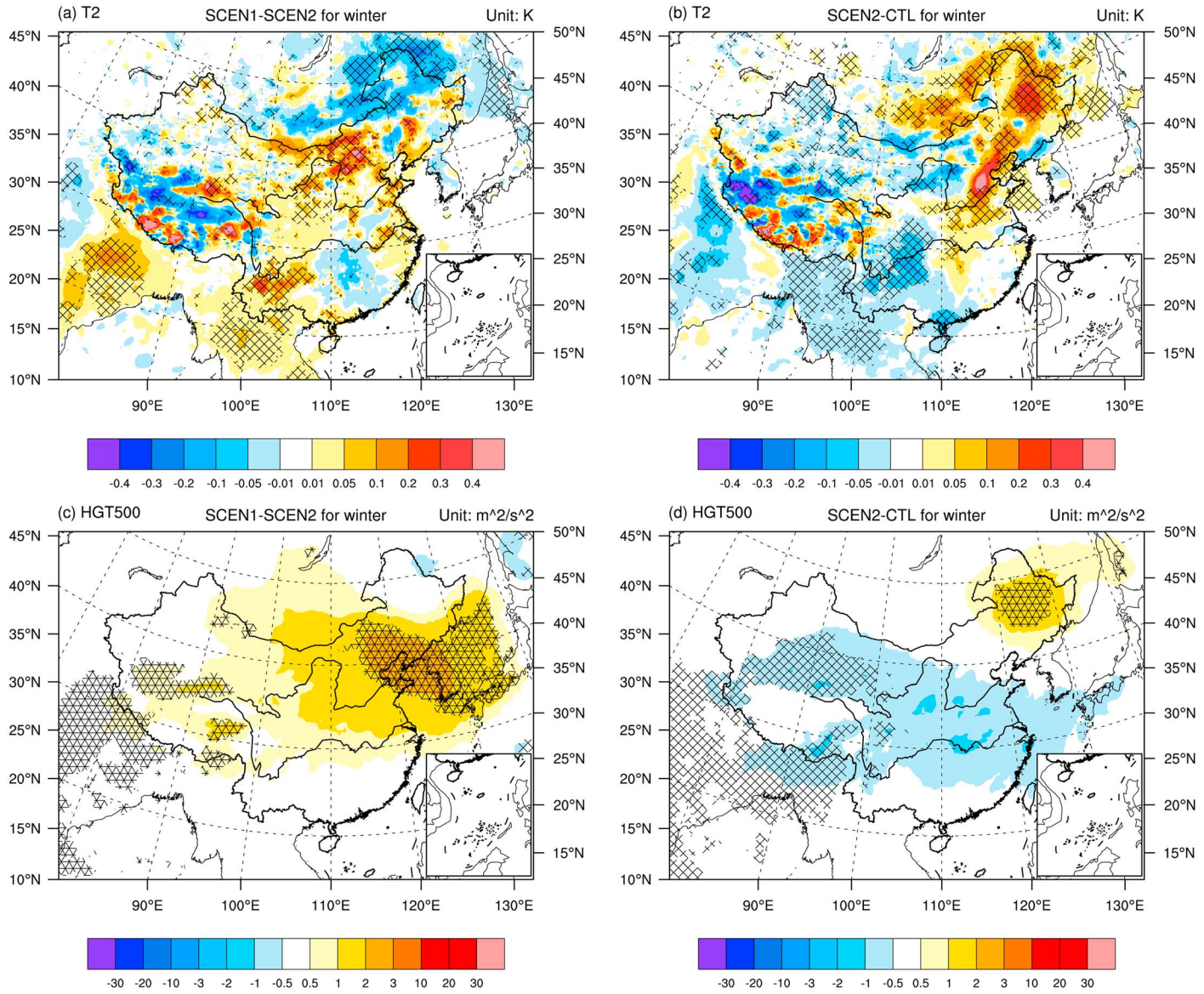

Figure 6. Mean differences in (a, b) 2-m temperature and (c, d) 500-hPa geopotential height caused by the (a, c) TKE source and (b, d) momentum sink in winter (December, January, and February). Regions with 95% confidence level of differences (calculated based on the contrast experiment t test formulation $t = \frac{\overline{d}}{s_D/\sqrt{n}}$) are highlighted with crosshatched lines.

(EAT) at 500 hPa could influence the East Asian winter monsoon, and the cold air in East Asia advances southeastward along the trajectories west of the EAT (L. Wang et al., 2009; Zhang et al., 1997). Therefore, this increase of HGT500 (Figure 4d) in winter could weaken the intensity of the EAT, which would inhibit the cold air sweeping across East Asia and cause the increase of 2-m temperature in northeast China (Figure 4b). The respective climatic impacts of momentum sink and TKE source are shown in Figure 6. According to Figures 6a and 6b, the increases of 2-m temperature in different areas may result from different components (momentum sink and TKE source) in wind turbine parameterization. The TKE source causes the increase of 2-m temperature over the inland of China (Figure 6a), whereas the momentum sink increases the 2-m temperature on the northeast of China (Figure 6b). For 500-hPa geopotential height, both momentum sink and TKE source tend to increase the 500-hPa geopotential height over the northeast China in winter. And the contributions of TKE source (Figure 6c) to the increase of 500-hPa geopotential height are larger than the contributions of momentum sink (Figure 6d).

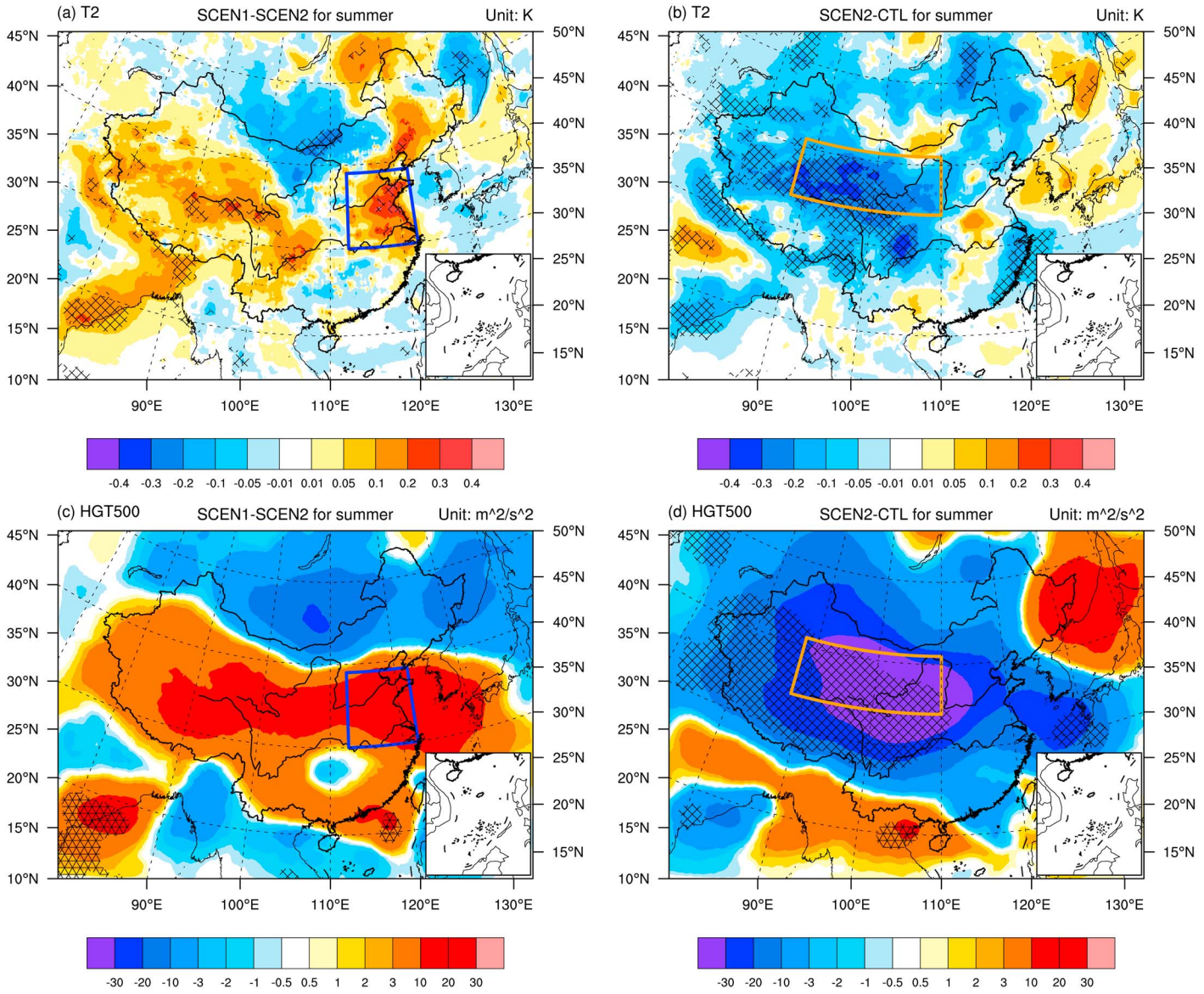

Figure 7. Mean differences in (a, b) 2-m temperature and (c, d) 500-hPa geopotential height caused by the (a, c) TKE source and (b, d) momentum sink in summer (June, July, and August). Regions with 95% confidence level of differences (calculated based on the contrast experiment t test formulation $t = \frac{\overline{d}}{s_D/\sqrt{n}}$) are highlighted with crosshatched lines.

In summer, the momentum sink and TKE source caused by wind farms are also separated to evaluate their respective contributions to regional climatic impacts of wind farms. Figure 7 shows the respective impacts of the momentum sink and TKE source on 2-m temperature and 500-hPa geopotential height in summer. The comparison between Figures 7a and 7b shows that the increase of temperature in the eastern coastal areas is mainly caused by the TKE source (blue boxes in Figures 4a and 7a); the decrease of temperature in the Chinese inland areas is mainly caused by the momentum sink (orange boxes in Figures 4a and 7b). We find that the increase of 500-hPa geopotential height and the increase of 2-m temperature caused by the TKE source are both located in the same areas (blue boxes in Figures 7a and 7c), and the decrease of 500-hPa geopotential height and decrease of 2-m temperature caused by the momentum sink both occur in the Chinese inland areas (orange boxes in Figures 7b and 7d). Because the western Pacific subtropical high (WPSH) at 500 hPa has an important influence on temperature in East Asia in summer, the increase of 500-hPa geopotential height (Figure 7c) caused by the TKE source could be conducive to the development of WPSH in

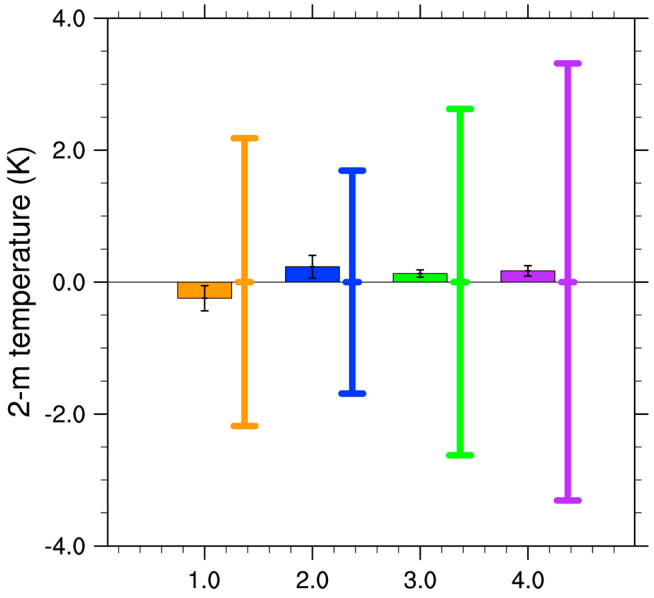

Figure 8. Regional averaged changes in 2-m temperature (colored bars) caused by the wind farms (SCEN1-CTL) in the selected areas (boxes 1.0–4.0 in Figures 4a and 4b) with 95% confidence intervals (shown as black line segments and calculated based on $\bar{d}_{0.05} = t_{0.05}(n) \times s_D/\sqrt{n}, \quad n = 48$). Twice the standard deviation of 2-m temperature (CTL) in corresponding selected areas in the same period (colored line segments).

summer, which would then cause the increase of 2-m temperature in the coastal area (Figure 7a); the decrease of 500-hPa geopotential height (Figure 7d) generated by the momentum sink could inhibit the WPSH from moving into East Asia, which would result in the decrease of 2-m temperature in the inland area (Figure 7b).

3.3. Evaluation on Climatic Impacts of Wind Farms

According to the analysis above, it can be concluded that the wind farms in the designed scenario, which represents the Chinese wind energy development level in 2015, have small impacts on regional climate. The impacts are considered small based on two aspects. First, the changes in many meteorological variables caused by wind farms are very small in most areas, and the statistically significant changes only occur in several specific areas where the changes are also limited (e.g., changes within ±0.5 K for 2-m temperature and within ±30 m^2/s^2 for 500-hPa geopotential height). Second, the impacts of wind farms on regional climate are much weaker than the interannual climate variability. Taking 2-m temperature as an example, several areas with extreme changes of 2-m temperature caused by wind farms (boxes in Figures 4a and 4b) are compared with the 2-m temperature interannual climate variability in the corresponding areas (Figure 8). The results show that the regional averaged changes of 2-m temperature caused by wind farms (shown by colored bars with a magnitude of 10^{-1}) are much smaller than the interannual climate variability of 2-m temperature (shown by colored line segments with a magnitude of 10^{0}). Similar results are also found in other meteorological variables. Moreover, we should not ignore the fact that wind energy plays an important part in slowing down the pace of global warming and protecting the environment by reducing fossil fuel combustion.

4. Conclusions and Discussion

Based on the Chinese wind farm information (number and locations of wind farms) from CWEA and Chinese cumulative wind power capacity data from Global Wind Energy Council, a new wind farm fleet scenario is designed to represent Chinese wind farm development level in 2015. The climatic impacts of wind farms studied in the article are intended to offer governments a scientific reference to support the environment-friendly development of wind energy.

The results suggest that wind farms under designed scenario could impact the local and regional climate in China, causing changes in both lower-level atmosphere (2-m temperature, 100-m horizontal wind speed, etc.) and upper-level atmosphere (500-hPa geopotential height, etc.) in several specific areas. In addition, the interactions between lower-level and upper-level atmospheric changes are fully discussed, which involve the EAT in winter and WPSH in summer.

Two main comparisons are carried out in the study: the comparison between two seasons (summer and winter) and comparison between two impacting factors (the momentum sink and TKE source). By comparing the impacts of wind farms in summer and winter, we found that the wind farms cause an increase of 2-m temperature in the eastern coastal area and a decrease in the Chinese inland areas in summer; the 2-m temperature mainly increases over a large area in winter. The slight positive anomaly in 500-hPa geopotential height caused by wind farms in winter passes 95% confidence level, whereas the changes in 500-hPa geopotential height caused by wind farms in summer, which are much larger than those in winter, do not pass 95% confidence level. By comparing the respective impacts of the momentum sink and TKE source on climate, we find that the momentum sink and TKE source sometimes play different roles in climatic impacts of wind farms, such as the increase of 500-hPa geopotential height (Figure 7c) caused by the TKE source and decrease of 500-hPa geopotential height (Figure 7d) caused by the momentum sink in summer. This study evaluates respective contributions of momentum sink and TKE source on wind farms' climatic impacts; ongoing work

will study the physical mechanism of how these two components (momentum sink and TKE source) impact the climate.

Our results show the impacts of wind farms on local and regional climate and the respective contributions of the momentum sink and TKE source in the wind turbine parameterization. However, there still exist several deviations between the climatic impacts of wind farms in our simulations and the climatic impacts of wind farms in reality. These deviations are generally caused by several factors, such as the inability of the wind farm data provided by CWEA to perfectly represent the actual wind farms in China (e.g., deserted wind farms and individual wind turbines could be neglected by the survey), the simplification used to represent wind farms in the simulations (e.g., same power curve applied in every wind turbine), and systematic deviations between model simulations and reality. In addition, it is known that the climatic impacts of wind farms increase as wind farm scale grows. Since wind farms under present development level are not in a very large scale, their climatic impacts are actually not so remarkable (compare Figures 4d and S1a in the supporting information) and could be easily influenced by other factors, such as using a different model or different wind turbine parameterization. Therefore, correct experimental procedure is of great importance in this kind of research, especially when the scale of wind farms is not large enough. And the statistical analysis is expected in a higher standard (higher confidence level means less possibility of random fluctuations) in the future research when the wind farms expand into a much larger scale (Figure S1).

Acknowledgments
We are thankful to the Chinese Wind Energy Association (CWEA) for providing the number and locations of Chinese wind farms. The detailed information about the Chinese wind farms used in this article is available from Table S1. The FNL reanalysis data set is available from https://rda.ucar.edu/datasets/ds083.2/. The ERL-Interim reanalysis data set is available from http://apps.ecmwf.int/datasets/data/interim-full-moda/levtype=sfc/. We are also thankful to Qifeng Qian for giving us advice on revisions to the article. This study is supported by the National Natural Science Foundation of China under grant 41475066 and Tsinghua University Initiative Scientific Research Program (grant 20131089357).

References

Baidya Roy, S., Pacala, S. W., & Walko, R. L. (2004). Can large wind farms affect local meteorology? *Journal of Geophysical Research*, *109*, D19101. https://doi.org/10.1029/2004JD004763

Baidya Roy, S., & Traiteur, J. J. (2010). Impacts of wind farms on surface air temperatures. *Proceedings of the National Academy of Sciences of the United States of America*, *107*(42), 17,899–17,904. https://doi.org/10.1073/pnas.1000493107

Barrie, D. B., & Kirk-Davidoff, D. B. (2010). Weather response to a large wind turbine array. *Atmospheric Chemistry and Physics*, *10*(2), 769–775. https://doi.org/10.5194/acp-10-769-2010

BP (2017). BP statistical review of world energy June 2017. Retrieved from https://www.bp.com/content/dam/bp/en/corporate/pdf/energy-economics/statistical-review-2017/bp-statistical-review-of-world-energy-2017-full-report.pdf

Chang, R., Zhu, R., & Guo, P. (2016). A case study of land-surface-temperature impact from large-scale deployment of wind farms in China from Guazhou. *Remote Sensing*, *8*(10). https://doi.org/10.3390/rs8100790

Fiedler, B. H., & Bukovsky, M. S. (2011). The effect of a giant wind farm on precipitation in a regional climate model. *Environmental Research Letters*, *6*(4), 045101. https://doi.org/10.1088/1748-9326/6/4/045101

Fitch, A. C., Lundquist, J. K., & Olson, J. B. (2013). Mesoscale influences of wind farms throughout a diurnal cycle. *Monthly Weather Review*, *141*(7), 2173–2198. https://doi.org/10.1175/MWR-D-12-00185.1

Fitch, A. C., Olson, J. B., Lundquist, J. K., Dudhia, J., Gupta, A. K., Michalakes, J., & Barstad, I. (2012). Local and mesoscale impacts of wind farms as parameterized in a mesoscale NWP model. *Monthly Weather Review*, *140*(9), 3017–3038. https://doi.org/10.1175/MWR-D-11-00352.1

Global Wind Energy Council (2017). Global wind report 2016: Annual market update. Retrieved from http://www.indianwindpower.com/pdf/GWEC_Global_Wind_2016_Report.pdf

Hasager, C. B., Vincent, P., Badger, J., Badger, M., Di Bella, A., Pena, A., et al. (2015). Using satellite SAR to characterize the wind flow around offshore wind farms. *Energies*, *8*(6), 5413–5439. https://doi.org/10.3390/en8065413

Skamarock, W. C., Klemp, J. B., Dudhia, J., Gill, D. O., Barker, D. M., Duda, M., et al. (2008). A description of the advanced research WRF version 3 NCAR Tech. Note 1–125

Smith, C. M., Barthelmie, R. J., & Pryor, S. C. (2013). In situ observations of the influence of a large onshore wind farm on near-surface temperature, turbulence intensity and wind speed profiles. *Environmental Research Letters*, *8*(3). https://doi.org/10.1088/1748-9326/8/3/034006

Vautard, R., Thais, F., Tobin, I., Breon, F. M., de Lavergne, J. G. D., Colette, A., et al. (2014). Regional climate model simulations indicate limited climatic impacts by operational and planned European wind farms. *Nature Communications*, *5*. https://doi.org/10.1038/ncomms4196

Wang, C., & Prinn, R. G. (2010). Potential climatic impacts and reliability of very large-scale wind farms. *Atmospheric Chemistry and Physics*, *10*(4), 2053–2061. https://doi.org/10.5194/acp-10-2053-2010

Wang, L., Chen, W., Zhou, W., & Huang, R. H. (2009). Interannual variations of east Asian trough axis at 500 hPa and its association with the East Asian winter monsoon pathway. *Journal of Climate*, *22*(3), 600–614. https://doi.org/10.1175/2008JCLI2295.1

Walsh-Thomas, J. M., Cervone, G., Agouris, P., & Manca, G. (2012). Further evidence of impacts of large-scale wind farms on land surface temperature. *Renewable and Sustainable Energy Reviews*, *16*(8), 6432–6437. https://doi.org/10.1016/j.rser.2012.07.004

Zhang, Y., Sperber, K. R., & Boyle, J. S. (1997). Climatology and interannual variation of the east Asian winter monsoon: Results from the 1979-95 NCEP/NCAR reanalysis. *Monthly Weather Review*, *125*(10), 2605–2619. https://doi.org/10.1175/1520-0493(1997)125%3C2605:CAIVOT%3E2.0.CO;2

Zhou, L. M., Tian, Y. H., Roy, S. B., Thorncroft, C., Bosart, L. F., & Hu, Y. L. (2012). Impacts of wind farms on land surface temperature. *Nature Climate Change*, *2*(7), 539–543. https://doi.org/10.1038/NCLIMATE1505